Research Article Open Access

Yao Chen, Weigang Zhu, Jianglin Wu, Yan Huang, Antonio Facchetti*, and Tobin J. Marks*

Recent Advances in Squaraine Dyes for Bulk-Heterojunction Organic Solar Cells

https://doi.org/10.1515/oph-2019-0001
Received April 1, 2019; accepted May 3, 2019.

Abstract: Squaraine (SQ) dyes are an important class of electron-donating (donors or p-type) semiconductors for organic solar cells (OSC) due to their facile synthetic access, broad optical absorption with high oscillator strengths, and chemical robustness. Blending them with compatible electron-acceptors (acceptors or n-type) yields OSC devices known as bulk-heterojunction (BHJ) small molecule donor organic solar cells (SMD-OSCs). Through extensive research on materials design, synthesis, characterization, and device optimization over the past five years, SMD-OSCs employing SQ-based structures have achieved remarkable increases in device power conversion efficiency (PCE), now approaching 8%. Although these PCEs have not yet equaled the performance of state-of-the art donor polymers and some other SMD semiconductors, SQ-based OSC progress highlights successful and generalizable strategies for small molecule solar cells that should lead to future advances. In this review, recent developments in SQ-based OSCs are discussed and analyzed.

Yao Chen, Weigang Zhu, Department of Chemistry and the Center for Light Energy Activated Redox Processes (LEAP), Northwestern University, 2145 Sheridan Road, Evanston, Illinois 60208, United States
Jianglin Wu, Yan Huang, Key Laboratory of Green Chemistry and Technology (Ministry of Education), College of Chemistry, Sichuan University, Chengdu 610064, P. R. China
***Corresponding Author: Antonio Facchetti,** Department of Chemistry and the Center for Light Energy Activated Redox Processes (LEAP), Northwestern University, 2145 Sheridan Road, Evanston, Illinois 60208, United States
Department of Materials Science and Engineering and the Center for Light Energy Activated Redox Processes (LEAP), Northwestern University, 2145 Sheridan Road, Evanston, Illinois 60208, United States
Flexterra Inc., 8025 Lamon Avenue, Skokie, Illinois 60077, United States
***Corresponding Author: Tobin J. Marks,** Department of Chemistry and the Center for Light Energy Activated Redox Processes (LEAP), Northwestern University, 2145 Sheridan Road, Evanston, Illinois 60208, United States

1 Introduction

During the past three decades, organic solar cells (OSCs) or organic photovoltaics (OPVs) have attracted considerable scientific and technological interest compared to conventional PV technologies based on traditional inorganic semiconductors [1–4] since printed, inexpensive, and mechanically flexible OSC/OPV modules can be fabricated on plastic substrates such as PET and PEN at low temperatures (< 120°C) using less capital intensive, high throughput roll-to-roll solution-process methodologies such as slot-dye, bar coating, and gravure/flexo printing [5–10]. The major OSC figure of merit, the power conversion efficiency (*PCE*) values of OSCs are now surpassing those of amorphous silicon and dye-sensitized cells, however, they remain significantly below those of mature crystalline silicon (Si) and cadmium-indium-gallium-sulfide (CIGS) technologies or recently disruptive solution-processed perovskite solar cell devices. However, since projected OSC modules do not contain toxic elements or require complicated/expensive vacuum-based fabrication processes, solar cells based on organic semiconductors continue to be a leading contender for inexpensive, ultra-light, and possibly optically transparent solar technology commercialization.

A blend of two semiconductors, an electron donor and an electron acceptor, forming a bulk heterojunction (BHJ), is the most common photoactive layer in OSCs. This layer is then sandwiched between two electrical contacts, one of them optically transparent and typically a transparent conducting oxide (TCO) such as ITO (tin-doped indium oxide) and a second electrode which could be either a metal, a conductve metal-oxide/conducting hybrid polymer, or a mesh of carbon nanotubes, metal nanowire, or

Department of Materials Science and Engineering and the Center for Light Energy Activated Redox Processes (LEAP), Northwestern University, 2145 Sheridan Road, Evanston, Illinois 60208, United States
Flexterra Inc., 8025 Lamon Avenue, Skokie, Illinois 60077, United States

graphene to cite just a few (Fig. 1). Additional charge (hole and electron) extracting interfacial layers are used to ensure efficient charge extraction, active layer-electrode cohesion, and thus to maximize PCE. Since groundbreaking discoveries informing the design for the two types of BHJ semiconductors [11–13], polymer donor+fullerene acceptor OSCs experienced great initial activity because fullerenes are commercially available, excellent electron-transporting semiconductors [14, 15], and enable optimal BHJ blend morphologies with many donor polymers [16–18]. Nevertheless, recent studies reveal that fullerenes also exhibit several drawbacks that may limit the long-term viability of the OSC field [14]. First, fullerenes and particularly those based on C_{60} (e.g., **$PC_{61}BM$**) have very poor optical absorption in the visible/NIR regions, thus limiting energy harvesting. Although C_{70}-based acceptors (e.g., **$PC_{71}BM$**) with superior optical cross- sections outperform C_{60} derivatives, they are too expensive for commercialization. Second, it is challenging to tune the molecular orbital energies of fullerenes since most have LUMO (lowest unoccupied molecular orbital) energies fixed near −4.0 eV, and laborious skeletal functionalization can only upshift the LUMO by ~250 meV at best [19]. Futhermore, most fullerenes are also unstable during OSC operation due to core dimerization reactions and/or morphological instability of the corresponding BHJ blend film [20–23].

To overcome the above limitations, a number of studies have addressed the development of non-fullerene OSCs (Figure 2). The first type of non-fullerene OSC was the so-called all-polymer solar cell (all-PSC) based on two semiconducting polymers with one functioning as the donor and the other as the acceptor. The second type of non-fullerene OSC was based on non-fullerene semiconducting small molecule acceptors (SMA-OSCs). Although the first example of non-fullerene BHJ OSCs was reported as early as 1995 [13], the development of this field was slow and mostly limited by the lack of high electron mobility polymeric or small molecular acceptors having optimal BHJ blend morphology. In 2007, an important breakthrough was made by Marder and coworkers who demonstrated an efficient all-polymer OSCs based on a novel polymeric acceptor [24], and the development of non-fullerene OSCs has accelerated since then [25]. The concurrent optimization of both structure and electronic characteristics of both donor and acceptor polymers could significantly enhance all-PSC performance metrics, now surpassing 11% for a binary single junction cell [26].

From a band structure point of view, all-PSCs provide the freedom to tune molecular orbital energy and topology and thus the optical absorption characteristics of both donor/acceptor polymers for optimal solar light harvesting [27]. Furthermore, from the charge transport perspective, acceptor polymers can potentially offer a more connected network for charge transport and potentially larger bulk electron mobilities than fullerene materials [28, 29] Finally, superior thermal, mechanical, and photo stability may be possible for all-PSCs [30–32]. Several families of acceptor polymers have been developed to date (Figure 2) with the most notable based on perylenediimide (PDI) [33], naphthalenediimide (NDI) [34], and azaacene skeletons containing boron-nitrogen coordination bonds [35, 36], with the NDI-based cells affording the greatest performance to date [37, 38].

Major advances in non-fullerene SMA OSCs were limited until about five years ago and mostly involved perylene diimide (PDI) acceptors with tunable architectures

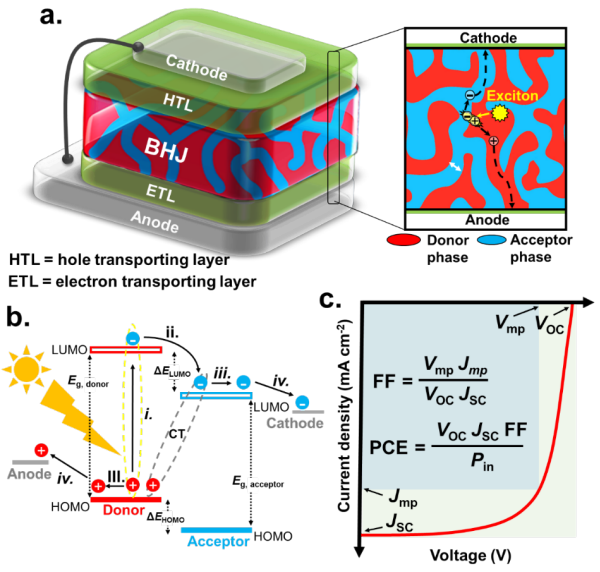

Fig. 1: Basic structure, operation, and performance parameters of an organic solar cell (OSC). (a) Structure of a bulk heterojunction (BHJ) OSCs. (b) Energy diagram of an OSC heterojunction showing the photon to charge conversion process with a photoexcitation energy equal the energy gap (E_g) of the donor: I) Under irradiation, an electron is photoexcited from the HOMO (highest-occupied molecular orbital) to the LUMO (lowest-unoccupied molecular orbital) of the donor forming an exciton (intramolecular hole-electron pair, yellow dash line). Note, the same process (not shown) occur in the acceptor; II) The exciton diffuses to the donor-acceptor interface, and the electron hops to the LUMO of the acceptor forming the charge transfer (CT) state (intermolecular hole-electron pair, gray dashed line); III) The CT dissociates into a free hole and electron, which move in the donor and acceptor domain, respectively; IV) The hole and electron are collected at the anode and cathode, respectively, to generate the photocurrent. (c) Current vs. voltage plot showing OSC figure-of-merits including short circuit current density, J_{SC}; open circuit voltage, V_{OC}, fill factor, FF, and the power conversion efficiency, PCE.

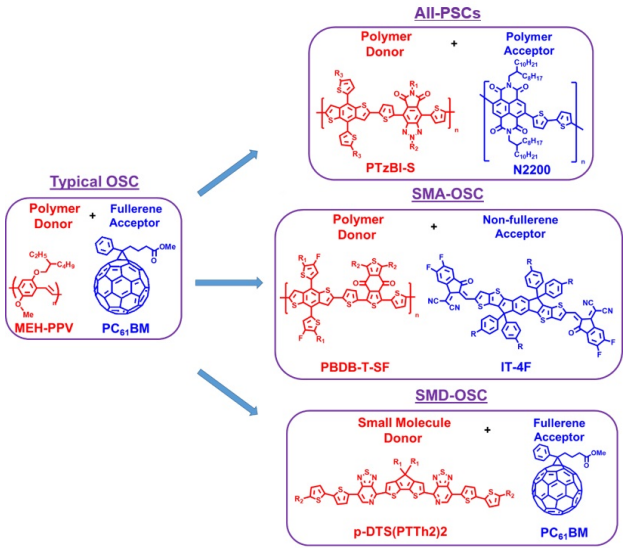

Fig. 2: Representative semiconductor components of different bulk-heterojunction (BHJ) organic solar cells (OSCs).

and electronic structures, with the highest PCEs typically less than ~4% [39–43]. Although PDIs are excellent electron-transporting semiconductors their pronounced tendency to aggregate/crystallize prevents optimal BHJ morphology formation due to excessively large domains formed (>1 μm in size) when blended with donor polymers [41]. For these reasons, breakthroughs followed by simultaneously suppressing PDI aggregation and retaining efficient electron transport characteristics, with PCEs reaching near 9% [44, 45].

Beyond the PDI acceptor family, the current state-of-the-art SMA family yielding even higher PCEs is that based on the 3,9-bis(2-methylene-(3-(1,1-dicyanomethylene)-indanone))-5,5,11,11-tetrakis(4-hexylphenyl)-dithieno[2,3-d:2′,3′-d′]-s-indaceno[1,2-b:5,6-b′]dithiophene (ITIC) molecular core (Figure 2) – a linear-shaped molecule end-functionalized with two electron-deficient groups and having sp^3-hybridized carbon atoms on the core to suppress excessive aggregation [46]. Such systems are π-conjugated and planar along the molecular axes, exhibit good electron mobilies, strong visible-NIR optical absorption, reoganization energies equal to or less than those of fullerenes, π-π packing coupling integrals rivaling or exceeding those of fullerenes, and tunable band gaps. More importantly, these ITIC OSCs can exhibit unusually low V_{OC} loss and ultra fast charge separation, offering the potential to drive OSC PCEs to new highs [47–50]. The recent development of ITIC-based SMAs demonstrates that both backbone and side chain engineering play an important role in tuning their absorption, energy levels and corresponding film morphological properties [51, 52]. The highest PCE achieved for a non-fullerene based solar cell has now surpassed 16% [53].

Far less explored are OSCs based on small molecule donor semiconductors (SMD-OSCs), with initial studies mostly involving vacuum-evaporated insoluble marterials such as acenes and phthalocyanines, and other linear and dentritic oligothiophenes enabling PCEs of ~ 2% [54, 55]. Advances have included the use of design rules employed in the NLO (nonlinear optics) literature, where the π-conjugated backbone consist of alternating multiple donor-acceptor (D-A) blocks, for efficient molecular orbital energetic tuning, red-shifting of the optical absorption, and morphology optimization when blended with fullerenes. Among the prominent D units include(benzo)-fused dithienosilole (DTS), benzodithiophene (BDT), and indacenodithiophene (IDT), while A moieties are typically diketopyrolopyrrole (DPP), fluorinated bezothiadiazole (F,-BT), and piridothiadiazole (PT). Most of these molecules are end-capped with electron acceptor units, as in the case of the SMA design, such as rhodamine-type and dicyanovinylene units. Blending these molecules with fullerenes has enabled PCEs as high as ~ 10% [56, 57] with recent breakthroughs for binary single junction SMD-OSCs surpassing 12% [57–59]. These results indicate important advances in small molecule materials design but also highlight the fact that these types of PSCs currently exhibit performance below that of state-of-the-art polymer-SMA OSCs. Nevertheless, lessons learned provide insight into broad applicability from solution to vapor-processed systems, chemical scalability, and tuning of electronic structure considering that both BHJ components are, in these systems, structurally well-defined. In this context, SMD materials based on squaraine cores are promising components for a further advances of the solar cell field as highlighted in the next section.

2 Brief History of SQ organic solar cells

Due to their intense, broad absorption bands in the visible and near infrared (NIR) regions, excellent photochemical and photophysical stability, and facile synthetic access, squaraine (**SQ**) dyes have attracted great attention for organic solar cells (OSCs) [60–67]. The evolution of the PCE for SQ for OSCs is displayed in Figure 3a and the molecular structures used in these studies are listed in Figure 3b. In 1976, Merritt et al. firstly used squaraine as photoactive layer for OSC devices, in which symmetric squaraine (SSQ) **1** was sandwiched between a transpar-

ent In_2O_3 anode and a metal (Ga) cathode using Schottky barrier-type cell [68]. However, due to the low dissociation efficiency of the photogenerated excitons only a modest power conversion efficiency (PCE) of 0.02% was reported. These poor early results probably discouraged OSC activity for squaraines and other materials, until the introduction of p-n junction/bulk heterojunction (BHJ) OSC architectures with fullerenes some years in the early 1990s.

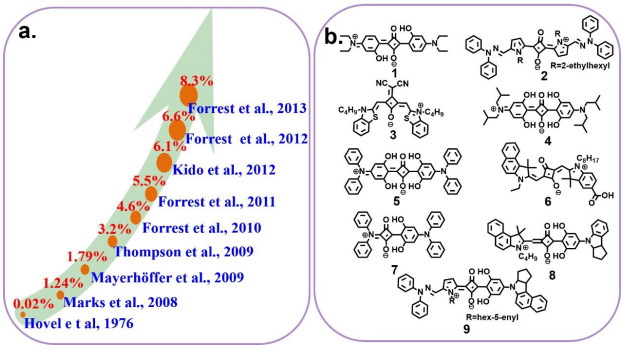

Fig. 3: (a) The evolution of the PCE for the indicated SQ-based organic solar cells, and (b) the molecular structures used in these studies.

An important milestone for SQ based OSCs was achieved by this laboratory in 2008, when for the first time a PCE > 1% was achieved for a SQ-based OSC [69]. Thus, branched alkyl chain substituents on the pyrrole impart good squaraine solubility which is essential for solution processing. Moreover, the film optical absorption is intense and broad (550-900 nm) which is an important prequesite for high-J_{SC} cells. A solution processed blend using the symmetric SQ dye **2** as the electron donor and $PC_{61}BM$ as the acceptor was used to fabricate a conventional device of structure of ITO/PEDOT:PSS /**2**:$PC_{61}BM$/LiF/Al. After this report, SQ based solar cell research accelerated. In 2009, Würthner et al. synthesized a series of central dicyanomethylene (diCN) substituted SQs such as structure **3** and fabricated cells with achieving a PCE of 1.79% with an impressive short-circuit current (J_{sc}) of 12.6 mA cm^{-2}, which was the highest J_{sc} value for small molecule OSCs at that time [70]. This study inspired a large community to work on SQ solar cells. Due to the strong light harvesting capacity in the vis-NIR regions and proper energetic levels, the symmetric SQ **4** became the most widely utilized material for OSC research. In 2009, Thompson et al. used the SQ **4** as the donor and C_{60} as the acceptor to fabricate planar heterojunction (PHJ) OSCs with a remarkable PCE of 3.2% [71]. The same group further enhanced the PCE of SQ **4**-based solar cells to 4.6% [72] and then 5.5% [73] using a BHJ architecture. In 2012, Kido et al. used the SQ **4** as donor and C_{70} as the acceptor to fabricate BHJ-OSCs devices by vacuum co-evaporation, which raised the PCE of SQ solar cells to 6.1% [74]. Furthermore, based on the SQ **4** structure, a series of symmetrical SQs were synthesized via side chain modification by Forrest et al. Among them, when employing SQ **5** as the donor and C_{70} as the acceptor to fabricate planar OSCs as the front subcell of a tandem device (back cell: SubPc: C_{70}), yielded a PCE of 6.6% [75].

Next, unsymmetrical SQs (USQs) began to receive greater attention in the OSC literature due to more effective tuning of the optoelectronic properties as well as enhanced solubility in common organic solvents. In 2009, Nüesch et al. first employed USQ **6** as the donor and C_{60} as the acceptor to fabricate planar solar cells [76]. Although the PCE was only 1%, the result stimulated the research interest in using USQs as OSC donor materials. Subsequently, Forrest et al. employed USQ **7** as the donor in a planar device with C_{60}, and obtained a PCE of 4.0% [77]. Tandem OSCs fabricated using the SSQ **5** and USQ **7** with C_{70} as the front planar cell and tetraphenyldibenzoperiflanthene (DBP) with C_{70} as the back planar cell achieved an excellent PCE of 8.3%, which remains the highest value of a SQ based OSC cells to date [78]. In the same year, Huang et al. first used arylamine and heterocyclic donor fragments in a series of USQs and fabricated solution-processed BHJ-OSCs with PCBM as the acceptor; these achieved PCEs near 4% [79, 80]. Following these results, additional efforts employing USQs **7** and **8** achieved similar performance [77, 81]. In 2015, by combining structural components developed in the work of Marks et al. [61], Huang et al. subsequently utilized hydrazone end-capped pyrrole and arylamine derivatives to develop a new USQ series. Among them, USQ **9** blended with PCBM resulted in BHJ-OSCs with PCEs of 4.35%, which was the highest reported value for solution-processed USQ-based cells at that time [82].

With tremendous efforts on materials design and synthesis as well as device optimization by the squaraine community, the PCEs of SQ-based OSCs have increased from 0.02% to 8.3% over the past decades. However, in comparison to state-of-the-art organic solar cells, the squaraine families still produce modest PCEs. In comparing the OSC metrics, the lower PCEs mainly originate from non-ideal FFs ($< \sim 0.50$) which can ascribed to the low hole mobility, generally $\sim 10^{-5} cm^2\ V^{-1}\ s^{-1}$ in the blend films. Increasing squaraine hole mobility is one key issue which should be addressed to enhance the PCEs of squaraine-based cells.

3 Synthetic Strategies for New SQ Dyes

Synthetic strategies for new photoactive squaraine dyes vary depending on the molecular structure desired since these molecules can be either symmetric (Figure 4, X = Y) and unsymmetric (Figure 4, X ≠ Y), as well as the chemical reactivity of the flanking end-groups [83–86]. Squaraine dye families containing 1,2-squarate derivatives and 1,3-squarate derivatives have been the most widely investigated for organic functional materials. For 1,2-squarate derivatives, synthetic routes usually use 3,4-dichlorocyclobutene-1,2-dione in an acylation reaction [65]. Several routes have been developed to synthesize the 1,3-squarate derivatives, however, the most common involves the condensation reaction of squaric acid with an (hetero)aromatic molecule possessing a nucleophilic site (Figure 4). This can originate from an electron-rich arene/heterocycle or upon deprotonation of an acidic functionality generating a carbanion. Thus, the most common end-groups consist of substituted alkyl anilines, phenols, pyrroles, indoles, and anhydrous bases. Thus, the synthesis of symmetrical squaraines simply consists of the reaction of one equiv. of squaric acid and two equivs. of a (hetero)aromatic reagent, typically in a refluxing alcohol (e.g., n-butanol), toluene, or benzene-alcohol mixtures. This widely used general synthetic method was developed by Sprenger et al. [87], where squaraine synthesis was carried out in an azeotropic solvent mixture containing 1-butanol and benzene. Optimization of this procedure was further developed by Law et al. [88], who found that this reaction in refluxing 2-propanol in the presence of ~3 reactantequiv. of tributylorthoformate enhances yields. The authors proposed that the major side reaction limiting the yield was esterification of the cyclobutenedione during the synthesis, and the use 2-propanol greatly suppresses this.

In contrast, unsymmetrical squaraine synthetic methodologies require multi-step reactions and typically afford poorer yields. Generally there are two synthetic routes to access unsymmetrical SQ dyes, specifically acylation with squaryl chloride or the reaction of squaric acid ester with an (hetero)aromatic reagent [89, 90]. However, similar to the synthetic routes to symmetric SQ dyes, these reactions are only efficient when using electron-rich (hetero)aromatic reagents. For those having electron-poor (hetero)-aromatic reagents, synthetic approaches to unsymmetrical SQs usually involve the use of organic lithium or tin compounds (See Figure 4 for details) [91–93]. Nevertheless, when compared to most other small molecule donors, the synthesis of SQs is more efficient and sustainable.

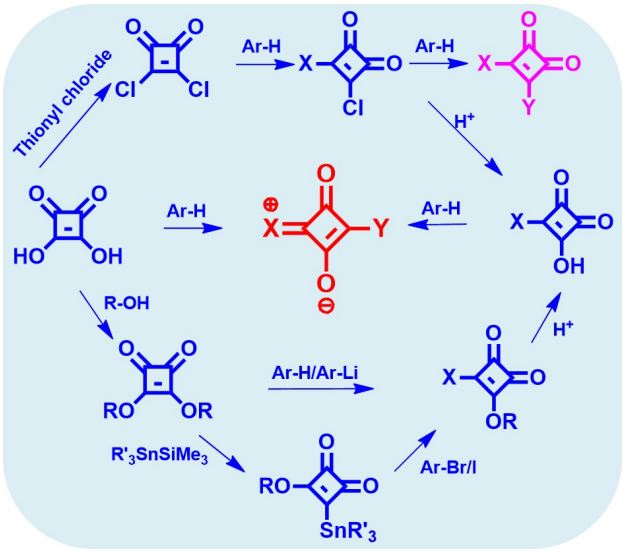

Fig. 4: Synthetic approaches to squaraine dyes.

4 Squaraines for binary BHJ solar cells

In this section the review focuses on progress in squaraine-based solar cells since 2015, including the development of novel squaraine structures (Figure 5) and their applications in binary solar cells (Table 1) [60]. In 2014 Huang et al. first used the indoline unit as the π-donor end-group for squaraines considering the electron-donating nature of this heterocycle, commercial availability, and facile functionalization [79]. A respectable PCE of 4.29% was demonstrated using squaraine **10** as electron donor and $PC_{71}BM$ as electron acceptor. Currently, most of the high-performance squaraines contain indoline as the key subunit. For example, Huang et al. developed many new indolines for implementation in squaraine-based solar cells [82, 94]. However, since indolines are strong electron donor units, they lead to SQs having a very high HOMO levels, yielding devices with low V_{OC} values. Thus, the HOMO level of structure **10** lies at −5.09 eV, so that using unsubstituted indoline as building block leads to OSCs with a V_{OC} of 0.82 V with $PC_{71}BM$ as the electron acceptor [79]. Lowering the electron donating capacity of the indoline unit is thus a promising strategy to enhance SQ solar cell performance. In 2015, Huang et.al implemented this strategy by functionalizing indoline with the strong electron withdrawing cyano (–CN) group [95].

Compared to the cyano-free squaraine **10**, SQ **11** shows comparable optical absorption in the film state with λ_{max} values of 633 nm and 718 nm, respectively. Additionally, the –CN substituent does not affect the BHJ film surface morphologies [95]. However, the cyano-substituted squaraine has a significantly far lower HOMO level (–5.20 vs. –5.09 eV), affording binary cells with far higher V_{OC} (0.93 vs. 0.83 V) as well as higher PCE metrics (5.24 vs. 4.22%) when paired with $PC_{71}BM$ as the acceptor. Interestingly, despite the lower HOMO, the SCLC data indicate that cyano-substituted squaraine **11** has higher hole mobility (4.00×10^{-5} cm^2 V^{-1} s^{-1}) than the cyano-free squaraine **10** (1.67×10^{-5} cm^2 V^{-1} s^{-1}). Density functional theory (DFT) calculations suggests that the higher hole mobility likely originates from CN-promoted intermolecular dipole-dipole interactions promoting close packing in the solid state. Another widely utilized electron withdrawing group is fluorine (F), which also has been widely used in the organic semiconductor literature [96]. In 2015, Huang et.al used a fluorine-substituted indoline and reported the new squaraines **12** and **13**. They reported that arene fluorination affects the intermolecular stacking patterns from x-ray analysis of single-crystals (Figure 6). The electron-donating indoline segment (D) is closely stacked with the electron-deficient squarate core (A, D···A packing pattern) for non-fluorinated **10**, while the fluorinated squaraine **13** has close π-π stacking between one molecular electron donating group (D) and electron donating group of an adjacent molecule (D') (D···D′ stacking pattern). The authors proposed that the D···D′motif promotes hole transport more effectively than a D···A packing pattern. Similar to the CN-substituted study discussed above, the new fluorine-substituted squaraines have lowered HOMO energy levels (–5.14 eV for **12** and –5.19 eV for **13**) and greater hole mobilities (6.80×10^{-5} cm^2 V^{-1} $s^{-1}$for **12** and 9.62×10^{-5} cm^2 V^{-1} s^{-1} for **13**) than those of **10** (4.81×10^{-5} cm^2 V^{-1} s^{-1}) [97]. Therefore, the OSCs fabricated with **12**/$PC_{71}BM$ and **13**/$PC_{71}BM$ blends exhibit higher PCEs (4.5% and 5.0%, respectively) than that of fluorine-free indoline-based squaraine **10** (4.0%). Note that the higher PCEs of 4.5% for **10**:$PC_{71}BM$, 5.0% for **12**:$PC_{71}BM$, and 6.04% for **13**:$PC_{71}BM$ were measured at elevated temperature (80°C; Figure 6c).

In 2018, this laboratory adopted a similar strategy by functionalizing squaraine **14** with fluorine at the 5 and 6 indolyl positions, resulting in the new fluorine-substituted squaraines **15** and **16**, respectively (Figure 5) [98]. These donor molecules exhibit, compared to the parent SQ **14**, a wider optical absorption (FWHM = 180 nm for **15** and 180 nm for **16**), lower HOMO energy levels (–5.28 eV for **15** and –5.28 eV for **16**), and slightly higher hole mobilities, 8.13×10^{-5} cm^2 V^{-1} $s^{-1}$for **15** and $8.91 \times$ cm^2 V^{-1} s^{-1} for **16**, as pristine thin films. The solar cells based on **15** and **16** exhibit almost identical V_{OC} (0.92 V) and PCE (4.6%) values at 25 °C, which are much larger than those based on fluorine-free squaraine **14**, 0.87 V and 4.2%, respectively. This study also revealed that the fluorine substituents lead to well-developed interconnected donor–acceptor networks in the blends as assessed by TEM. In 2015, Ko et al. reported similar results using a different electron withdrawing group (cyanoacetate) in SQ **17** (Figure 5) [99]. The authors reported that this squaraine also exhibits a broad optical absorption band (∼ 600 nm - ∼ 800 nm) as well as a relatively low HOMO energy level (–5.086 eV). Solar cells of structure ITO/PEDOT:PSS/**17**:$PC_{61}BM$/Al exhibit a PCE of 5.25% (J_{SC} = 11.86 mA cm^{-2}, V_{OC} = 0.82 V and FF = 0.54), with performance limited by the poor FF.

The data discussed above reveal that SQ OSC performance is greatly limited by the poor FF values (typically < 0.5), reflecting the low squaraine bulk hole mobility. Thus, a possible route to improve the device performance is to enhance carrier mobility by extending the SQ molecular core [100, 101], since enlarging π-conjugation in organic semiconductors usually favors charge transport [94, 102]. Indeed, in 2016, Kido *et al.* reported bi-squaraine small molecule donor **20** having a A-D-A-structure. A key D component of this SQ is the benzo[1,2-b:4,5-b'] dithiophene (BDT) unit, which is used to connect two squaric rings (Figure 5). In comparison to traditional squaraines such as **18** and **19**, newly developed bi-squaraine **20** shows a one order of magnitude enhanced hole mobility in blend films with the $PC_{71}BM$ acceptor, 1.14×10^{-4} for **20** vs. $2.60 \times 10^{-5}$$cm^2$ V^{-1} s^{-1} for **18** vs. $2.40 \times 10^{-5}$$cm^2$ V^{-1} s^{-1} for **19**. The OSCs based on **20** exhibit a much higher PCE (5.75%) than those based on the traditional squaraines, 3.82% for **18** and 4.11% for **19**, achieved without post-film deposition treatments. Furthermore, the PCEs of these devices were enhanced with simple thermal annealing at 80°C for 15 min, yielding a respectable PCE of 6.33%. Note, that the FF of these cells is also greatly improved, surpassing 0.52, which is higher than those achieved previously in squaraine-based BHJ solar cells (typically far less than 0.50). Again, greater PCEs (5.5% for **18**:$PC_{71}BM$, 5.8% for **19**:$PC_{71}BM$, 7.4% for **20**:$PC_{71}BM$) were measured at 80°C cell operation temperature. Inspired by this exciting result, Kido et al. further developed new bi-squaraines employing the rigid and planar indacenodithieno[3,2-b]thiophene (IDTT) as connecting unit in place of BDT [94]. New bi-squaraine **21** (Figure 5) exhibits a molar extinction coefficient ($\epsilon_r = 2.84 \times 10^5$ M^{-1} cm^{-1}) and wide optical absorption band (∼ 550 - ∼ 850 nm) in solution, which is important for enhancing OSC J_{SC} and PCE. Furthermore, this

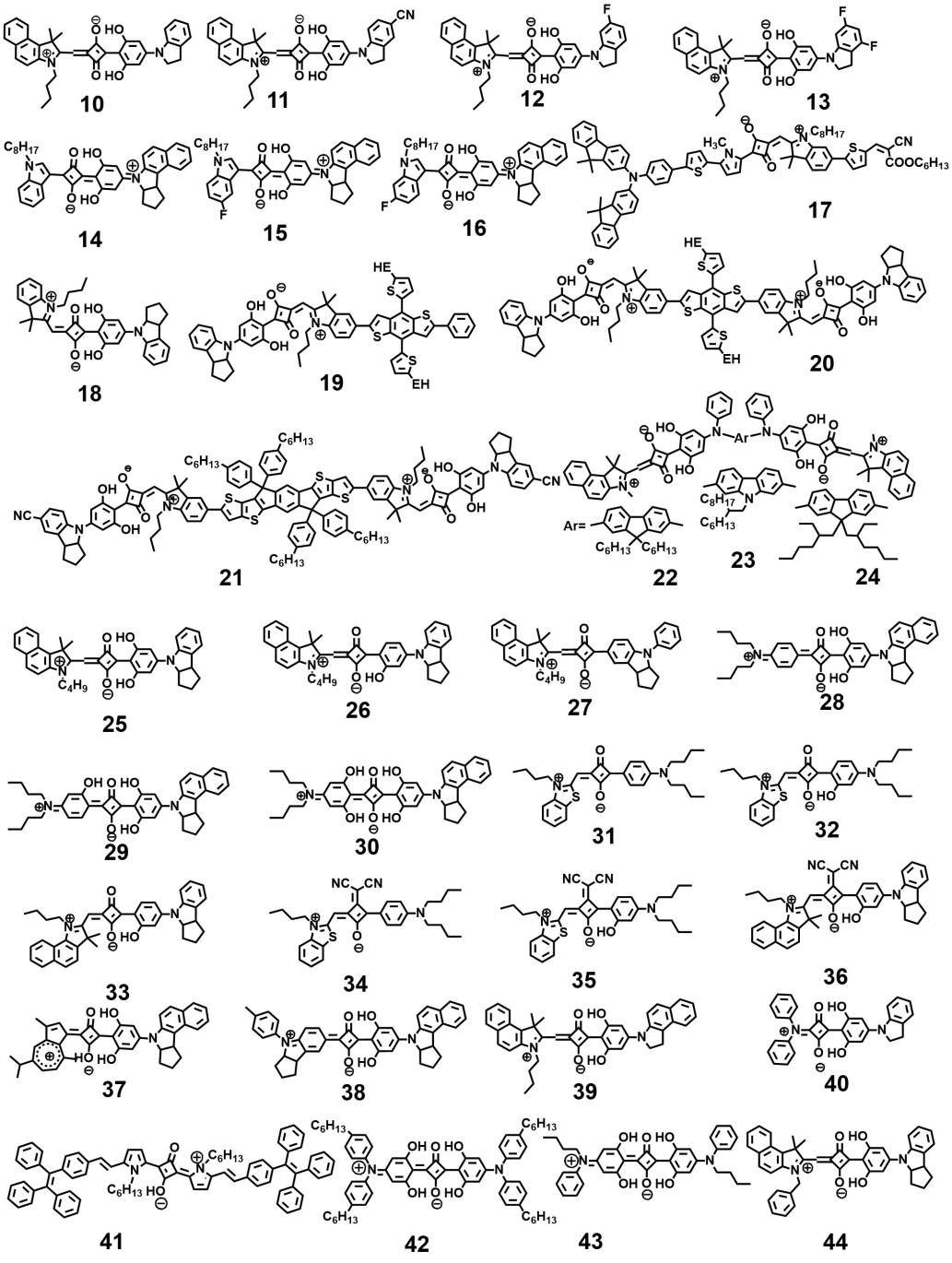

Fig. 5: Structures of squaraine-based small molecules used as donor semiconductors in OSCs.

dye has a favorable HOMO energy of −5.20 eV as well as an excellent hole mobility as high as 2.51×10^{-4}cm^2 V^{-1} s^{-1}. A BHJ OSC of structure ITO/ MoO_3/**21**: $PC_{71}BM$ / BCP /Al produces a high PCE of 6.65% (J_{SC} = 13.34 mA cm^{-2}) with a promising FF of 0.53 and a high V_{OC} of 0.94 V. After thermal annealing the blend at 90 °C for 10 min, the PCE is further increased to 7.05% (J_{SC} = 14.03 mA cm^{-2}, V_{OC} = 0.93 V and FF = 0.54), which was the highest PCE for squaraine-based solar cells at that time. More recently, Li et al. reported butterfly-shaped unsymmetrical squaraine dimers, **22-24** (Figure 5) using the bi-squaraine strategy [103]. The author selected fluorene and carbazole moieties as the bridging units and used 1,1,2-trimethyl-1*H*-benzo[e]indole as end groups. Upon side-chain modification of the fluorene moiety, a PCE of 4.38% (J_{SC} = 10.82 mA cm^{-2}, V_{OC} = 0.83 V and FF = 0.49) was achieved for **23**:$PC_{71}BM$ -based solar

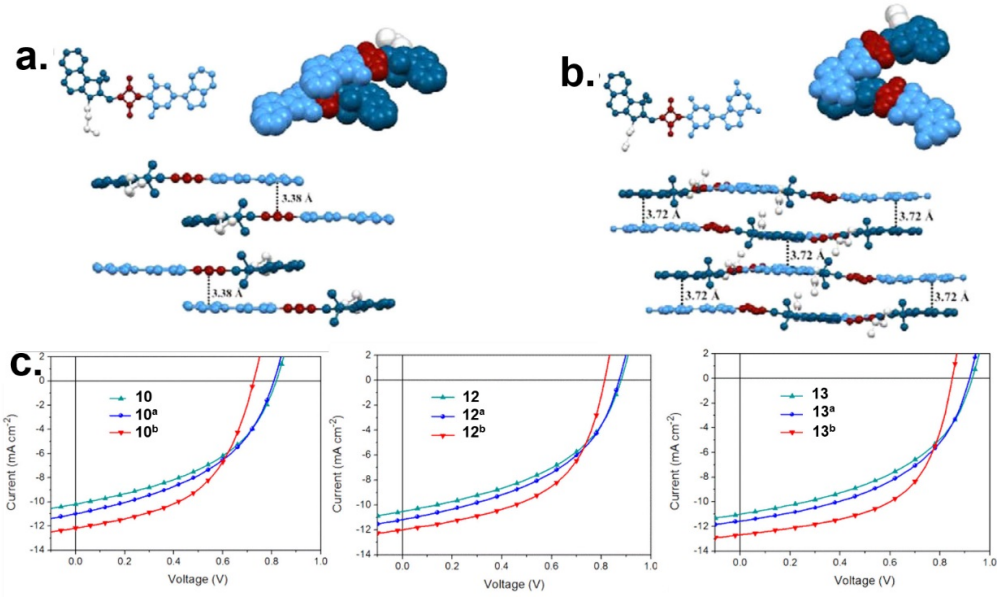

Fig. 6: Crystal packing of squaraines (a) **10** and (b) **13**, and (c) OSC *J-V* plots for **10**:$PC_{71}BM$, **12**:$PC_{71}BM$, **13**:$PC_{71}BM$ solar cells after thermal annealing at 80 °C, 10 min; cells measured at 80 °C [97]. Reprinted with permission from Ref. [97]. Copyright 2015 American Chemical Society.

cells. The performance of these cells is limited to ∼ 4% mostly because of the modest J_{SC} (7.22–10.19 mA cm^{-2}) and FF (0.39-0.49).

Several studies on squaraine dyes have shown that hydroxyl-substitution of the phenyl group near the squaraine core can considerably affect key structural and opto-electronic properties such as intermolecular stacking, optical/emission characteristics, energy levels as well as a OSC performance [60]. Recent studies suggest that squaraine hydroxyl substitution consistently enhances solar cell performance versus the OH unsubstituted materials as initially reported by Kido et al in 2014 [104]. In 2017, Huang et al. reported a family of hydroxyl-substituted unsymmetric squaraines, **25**-**27** (Figure 5) consisting of 1,2,3,3a,4,8b-hexahydrocyclopenta[b]indole with different -OH substitution levels on the phenyl. OSCs of structure ITO/MoO_3 (8 nm)/ USQ:$PC_{71}BM$ (65 nm)/LiF (0.7 nm)/Al (100 nm) exhibit similar trends with previous reports–that is increasing phenyl group hydroxy-substitution leads to higher PCEs, i.e., 4.0 % for **25**, 2.8% for **26**, 1.1% for **27**. More recently, the same group investigated OH-substituted unsymmetrical squaraines **28-30** (Figure 5) consisting of 7,7a,8,9,10,10a-hexahydro-benzo[e]cyclopenta[b]indole as the electron donating group [105]. Similar to previous reports it was found that increasing the number of OH groups from two in **28** to three in **29** affords higher device performance, PCE = 5.34 and 6.07%, respectively (Figures 7a, 7b). However, further increasing to four OH groups in squaraine **30** lowers the power conversion efficiency to 5.67%, which reflects erosion of the hole mobility. Furthermore, despite the fact that these blends show similar uniform surface morphologies with small RMS roughnesses of 0.23–0.37 nm, TEM characterization indicates that the **29**:$PC_{71}BM$ films have the smallest phase separation length scales versus the **28**:$PC_{71}BM$ and **30**:$PC_{71}BM$ blends, which apparently correlates with greater charge separation efficiency at the D/A interface (Figure 7c). In summary, these studies demonstrate that hydroxy substitution can inform the design of new high-performance SQ structures for OSCs.

Another informative structural variation in the squaraine structure is achieved by replacing one squaric core oxygen atom with an electron-deficient group such as dicyanomethylene. As noted in the previous section, a large J_{SC} of 12.6 mA cm^{-2} is achieved using an additional dicyanovinyl acceptor moiety at the central acceptor portion of SQ structure **3** (Figure 5) [70]. Interestingly, the single-crystal diffraction-derived structure of **3** indicates that this squaraine is planar and crystallizes with a close π-π interplanar stacking distance of 3.4 Å (Figure 8a), which is important for efficient exciton diffusion and carrier transport. However, a low V_{OC} of 0.31 V was achieved leading to a modest PCE of 1.79%. Nevertheless, this finding offers an extremely important design strategy to increase PCE. Thus, Huang et al. systematically investigated the effects of dicyanomethylenation by synthesizing

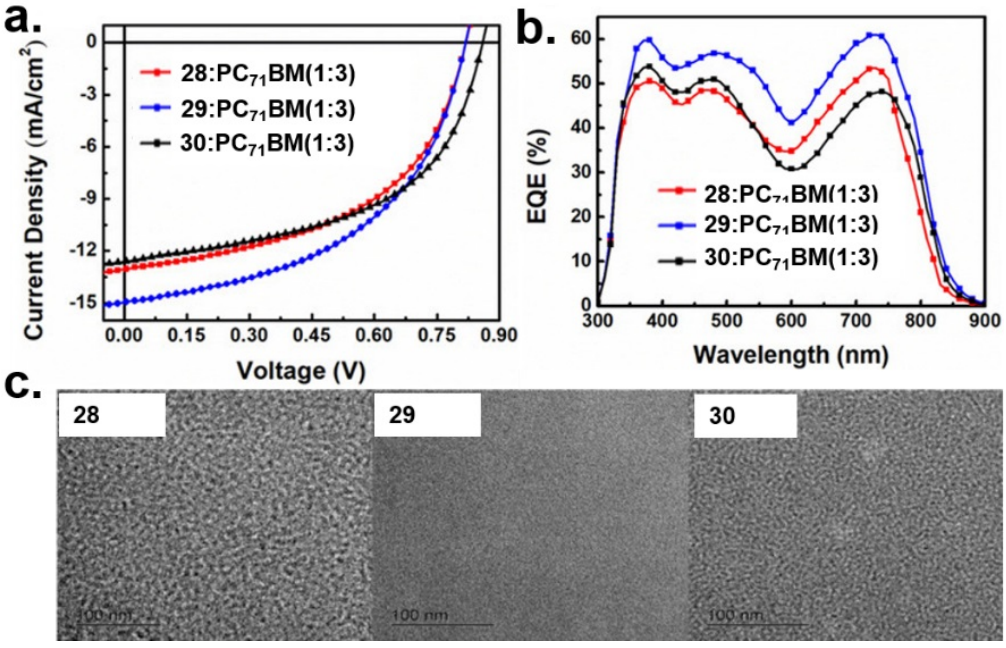

Fig. 7: a) *J-V* characteristics of the three SQ (**28**, **29**, **30**):$PC_{71}BM$ OSCs, b) External quantum efficiency (EQE) of the three SQ:$PC_{71}BM$ (1:3) devices, c) TEM images of the SQ:$PC_{71}BM$ (1:3) active layers [105]. Reprinted with permission from Ref. 105. Copyright 2018 Wiley-VCH.

squaraines **31**-**36** (Figure 5) and characterizing their physical properties and device performance [106]. The results indicate that the presence of the dicyanomethylene groups on the central squaric ring lowers the optical bandgap by ~ 0.06–0.11 eV and deepens the HOMO energy from ~ −4.88 to ~ −5.02 eV in **31-33,** and to −4.97 to ~ −5.11 eV in **34-36**. Furthermore, DFT computations suggest that =O => $=(CN)_2$ substitution increases the dipole moment and reverses the dipole moment direction. Also, in TEM images, the $=(CN)_2$ substituted squaraine blends of **34**-**36** with $PC_{71}BM$ display much smaller phase separation dimensions than the corresponding =O squaraine blends with **31-33** (Figure 8e). Moreover, dicyanomethylenation affects the π-π stacking patterns of **32** and **35** as accessed from single crystal diffraction analysis (Figure 8b). Thus, SQ **32** without dicyanomethylenation exhibits a head-to-tail molecular arrangement to form a staircase-type J-dimer (J-aggregate characteristics), while **35** with dicyano-methylenation aggregates in an antiparallel fashion to form a sandwich-type arrangement (H-dimer; Figures 8d, 8e). Solution-processed BHJ-OSCs using $PC_{71}BM$ as the acceptor show that $=(CN)_2$ substituted SQs **34**-**36** exhibit higher J_{SC} (6.51 – 10.89 mA cm^{-2}) and V_{OC} values (0.61 – 0.87 V), and thus higher PCEs (1.46% - 4.58%) than their parent counterparts **31**-**33** where J_{SC} = 3.02 – 8.67 mA cm^{-2}; V_{OC} = 0.41 – 0.78 V; PCE = 0.45 – 3.05%.

Developing/introducing new building blocks is a common route to achieve high-performance organic semiconductors, including for squaraines. Recently, there have been many new electron donor moieties implemented in squariaines, resulting in structures (e.g. **37**-**40**, Figure 5) with enhanced device performance. A low bandgap (1.38 eV) squaraine dye (**37**) consisting of guaiazulene as an electron donating group shows an hole mobility up to 1.25× 10^{-4}cm^2 V^{-1} s^{-1}. BHJ-OSC of structure ITO/ MoO_3/**37**: $PC_{71}BM$ / BCP /Al using $PC_{71}BM$ as acceptor exhibit a PCE of 2.23% with a high V_{OC} of 0.79 V [107]. With an indoline derivative directly link to the squaric core as an electron donating group (**38**), BHJ-OSC of structure ITO/ MoO_3/**38**: $PC_{71}BM$/BCP /Al using $PC_{71}BM$ as acceptor exhibit a PCE of 5.49% with a high V_{OC} of 0.83 V (J_{SC} = 13.50 mA cm^{-2}; FF = 0.49) [111]. A higher PCE (5.35% vs. 4.29%) was achieved when the squaraine consisting of 3*H*-benzo[e]indoline as electron donor (**39**) than that squaraine **10** consisting of indoline enables extended π-conjugation [112]. With the nitrogen of the core as an electron-donating group, the new squaraine **40** exhibits a PCE of 4.04% with a high V_{OC} of 1.04 V, J_{SC} = 9.48 mA cm^{-2}, and FF = 0.41, when combined with $PC_{71}BM$ in the OSC of structure ITO/ MoO_3/**40**: $PC_{71}BM$/BCP /Al [113].

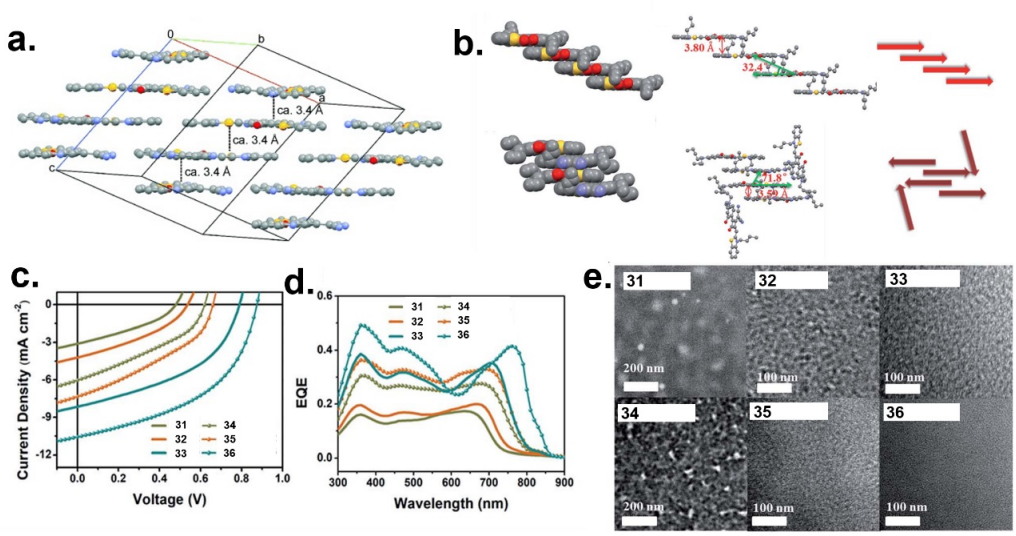

Fig. 8: (a) Spatial arrangement of squaraine **3** in the crystal lattice. Reprinted with permission from Ref. [70]. Copyright 2009 Wiley-VCH), b) Single crystal structures of squaraines **32** (top) and **35** (bottom), c) TEM images of the active layers of the indicated squaraine BHJ blends with $PC_{71}BM$; sqauaraine numbering as in Figure 5. Reprinted with permission from Ref. 106. Copyright 2018 The Royal Society of Chemistry).

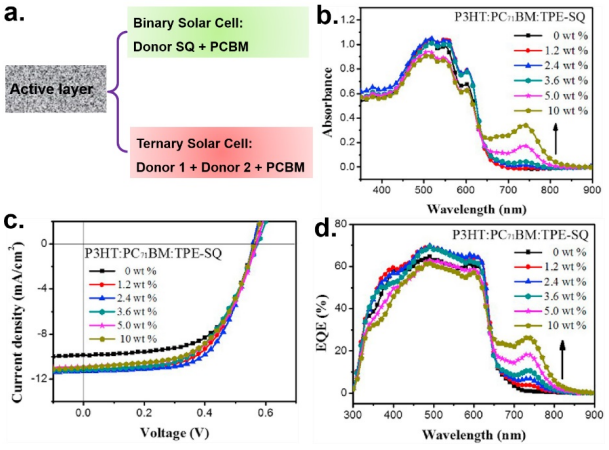

Fig. 9: (a) Active layer compositions in the indicated binary/ternary squariane solar cells, (b) UV-vis absorption spectra of P3HT:$PC_{71}BM$:TPE-SQ films as a function of the TPE-SQ doping concentration, (c) *J*-V, and (d) EQE vs. wavelength characteristics with different concentrations of TPE-SQ in P3HT:$PC_{71}BM$:TPE-SQ based ternary solar cells [128]. Reprinted with permission from Ref. 128. Copyright 2016 Elsevier

5 Recent developments in ternary solar cells based on squaraine (SQ) dyes

Ternary solar cells are OSCs where the photoactive layer is comprised of a mixture of three organic semiconductors (Figure 9a). Using this combination allows broadening of the light harvesting, tuning the BHJ nanomorphology, and sometimes promoting carrier mobility, thereby enhancing key OSC metrics [114–116]. Most reported SQ-based ternary solar cells since 2015 were fabricated adding SQ as the third component in fullerene-based binary blends, and optimized PCEs are mostly ~ 5% (Table 2) [117–126]. In 2015, Zhang and co-workers [127] reported ternary OSCs based on the narrow bandgap polymer donor poly{[4,9-dihydro-4,4,9,9-tetra(4-hexylbenzyl)-s-indaceno[1,2-b:5,6-b0]-dithiophene-2,7-diyl]-alt-[2,3-bis(3-(octyloxy)phenyl)-2,3-dihydro-quinoxaline-2,20-diyl] (PIDTDTQx) with $PC_{71}BM$ as the acceptor, and using as the third donor component squaraine **4**. PIDTDTQx exhibits a wide absorption wavelength range from 300 nm to 650 nm while **4** shows the maximum absorption around 700 nm, and therefore, complementary to that of $PC_{71}BM$. Solar cells having the blends PIDTDTQ$x_{(100-y)}$:**4**$_y$:$PC_{71}BM$ with the y values ranging from 0 to 15 wt% were investigated. For conventional ITO/PEDOT:PSS/Active Layer/PFN/Al device structures, the blend having 9 wt% **4** exhibits the best performance with a PCE of 6.49%, V_{OC} of 0.85 V, J_{SC} of 11.56 mA/cm^2 and FF of 0.66 (Figures 9b, 9c, 9d) [120]. This result is greatly improved compared to the binary PIDTDTQx:$PC_{71}BM$ (PCE = 5.47%) and **4**:$PC_{71}BM$ (PCE = 1.78%) cells. To understand why the addition of **4** to the polymer blend enhances performance, the authors carried out photoluminescence (PL) spectroscopy, time-resolved transient photoluminescence (TRTPL)

Table 1: Photovoltaic Performance data for Squaraine-based BHJ-OSCs

Device Structure	V_{oc} (V)	J_{sc} (mA cm^{-2})	FF	PCE (%)	Ref.
Ga/**1**/In_2O_3	/	/	0.20	0.02	[68]
ITO/PEDOT:PSS /**2**:$PC_{61}BM$/LiF/Al	0.62	5.70	0.35	1.24	[69]
ITO/PEDOT:PSS /**3**:PCBM/Ca /Al	0.31	12.6	0.47	1.79	[70]
ITO/ MoO_3/**4**: $PC_{71}BM$/ C_{60}/BCP /Al	0.92	12.0	0.50	5.2	[108]
ITO/**5**/ C_{60}/BCP /Al	0.82	6.71	0.59	3.2	[109]
ITO/PEDOT:PSS /**6**/ C_{60} /Alq_3/Al	0.38	5.0	0.31	0.59	[76]
ITO/MoO_3 /**7**/ C_{60} /PTCBI/Al	0.92	6.3	0.63	3.7	[77]
ITO/ MoO_3/**8**: $PC_{71}BM$/LiF /Al	0.81	10.19	0.48	3.9	[110]
ITO/ MoO_3/**9**: $PC_{71}BM$/LiF /Al	0.78	11.80	0.45	4.12	[82]
ITO/ MoO_3/1**0**: $PC_{71}BM$/LiF /Al	0.81	11.03	0.48	4.29	[80]
ITO/ MoO_3/**11**: $PC_{71}BM$ / BCP /Al	0.92	11.38	0.50	5.24	[95]
ITO/ MoO_3/**12**: $PC_{71}BM$ / C_{70} / BCP /Al	0.87	11.18	0.46	4.47	[97]
ITO/ MoO_3/**13**: $PC_{71}BM$ / C_{70} /BCP /Al	0.92	11.56	0.47	5.00	[97]
ITO/ MoO_3/**14**: $PC_{71}BM$/LiF /Al	0.87	11.72	0.41	4.18	[98]
ITO/ MoO_3/**15**: $PC_{71}BM$/LiF /Al	0.92	12.08	0.42	4.65	[98]
ITO/ MoO_3/**16**: $PC_{71}BM$/LiF /Al	0.92	11.21	0.44	4.66	[98]
ITO/PEDOT:PSS /**17**:$PC_{61}BM$ /Al	0.82	11.86	0.54	5.25	[99]
ITO/ MoO_3/**18**: $PC_{71}BM$ / BCP /Al	0.85	11.53	0.44	4.31	[101]
ITO/ MoO_3/**19**: $PC_{71}BM$ / BCP /Al	0.93	11.65	0.44	4.77	[101]
ITO/ MoO_3/**20**: $PC_{71}BM$ / BCP /Al	0.91	13.38	0.52	6.33	[101]
ITO/ MoO_3/**21**: $PC_{71}BM$ / BCP /Al	0.93	14.03	0.54	7.05	[94]
ITO/ MoO_3/**22**: $PC_{71}BM$ / BCP /Al	0.81	7.22	0.39	2.26	[103]
ITO/ MoO_3/**23**: $PC_{71}BM$ / BCP /Al	0.83	10.82	0.49	4.38	[103]
ITO/ MoO_3/**24**: $PC_{71}BM$ / BCP /Al	0.84	10.19	0.47	4.02	[103]
ITO/ MoO_3/**25**: $PC_{71}BM$ / LiF/Al	0.81	10.19	0.48	3.9	[110]
ITO/ MoO_3/**26**: $PC_{71}BM$ / LiF /Al	0.74	8.65	0.44	2.80	[110]
ITO/ MoO_3/**27**: $PC_{71}BM$ / LiF /Al	0.60	4.76	0.39	1.10	[110]
ITO/ MoO_3/**28**: $PC_{71}BM$ / BCP /Al	0.83	13.13	0.49	5.34	[111]
ITO/ MoO_3/**29**: $PC_{71}BM$ /Liq /Al	0.82	14.95	0.50	6.07	[105]
ITO/ MoO_3/**30**: $PC_{71}BM$ /Liq /Al	0.86	12.58	0.52	5.67	[105]
ITO/ MoO_3/**31**: $PC_{71}BM$ / BCP /Al	0.41	3.02	0.37	0.45	[106]
ITO/ MoO_3/**32**: $PC_{71}BM$ / BCP /Al	0.50	4.13	0.37	0.77	[106]
ITO/ MoO_3/**33**: $PC_{71}BM$ / BCP /Al	0.78	8.67	0.45	3.05	[106]
ITO/ MoO_3/**34**: $PC_{71}BM$ / BCP /Al	0.61	6.51	0.37	1.46	[106]
ITO/ MoO_3/**35**: $PC_{71}BM$ / BCP /Al	0.65	7.75	0.38	1.91	[106]
ITO/ MoO_3/**36**: $PC_{71}BM$ / BCP /Al	0.87	10.89	0.49	4.58	[106]
ITO/ MoO_3/**37**: $PC_{71}BM$ / LiF /Al	0.79	6.81	0.41	2.23	[107]
ITO/ MoO_3/**38**: $PC_{71}BM$ / LiF /Al	0.83	13.50	0.49	5.49	[111]
ITO/ MoO_3/**39**: $PC_{71}BM$ / BCP /Al	0.73	15.64	0.47	5.35	[112]
ITO/ MoO_3/**40**: $PC_{71}BM$ / BCP /Al	1.04	9.48	0.41	4.04	[113]

spectroscopy, space-charge-limited current (SCLC), and atomic force microscopy (AFM) measurements. The PL intensity of PIDTDTQx is considerably quenched as the **4** content increases, indicating energy or charge transfer (CT) from PIDTDTQx to **4**. TRTPL spectroscopy results show that excitons in PIDTDTQx and **4** can be effectively quenched by each other and CT may occur between PIDTDTQx and **4**. Single carrier diodes were also fabricated using ITO/PEDOT:PSS/active layer/MoO_3/Ag as hole-only and Al/LiF/active layer/LiF/Al as electron-only devices, respectively, and mobilities were estimated by the SCLC model. For the ternary solar cells with 9 wt% of **4**, the hole and electron mobilities are more balanced with a μ_h/μ_e value of 1.34. Therefore, the main contributors to the increased PCEs of the ternary solar cells are the enhanced photon harvesting, CT between PIDTDTQx, and **4** and more balanced charge transport.

In 2016, the Wu group [128] synthesized new near-infrared (NIR) absorbing squaraine derivative **41**, and investigated the effect of adding it to a conventional P3HT:$PC_{71}BM$ binary OSC. **41** exhibits a strong NIR absorption from 600 to 800 nm, and the highest occupied molecular orbital (HOMO) and the lowest unoccupied molecular orbital (LUMO) are positioned between the corresponding levels of P3HT and $PC_{71}BM$. The complementary optical absorption (Figure 9b) and cascade energy levels suggest that **41** as the third component is promising to further increase P3HT:$PC_{71}BM$ solar cell performance. As a control cell, the binary P3HT:$PC_{71}BM$ blend has a V_{OC} of 0.56 V, a J_{SC} of 9.90 mA/cm^2,a FF of 0.60, and a PCE of 3.33%. The highest PCE of 3.93% with V_{OC} of 0.56 V, J_{SC} of 11.32 mA/cm^2 and FF of 0.62 was achieved for the ternary blend having 2.4 wt% of **41** (Figures 9c, 9d). To investigate how **41** affects BHJ blend film morphology, AFM and X-ray diffraction (XRD) measurements were performed. AFM images show that the ternary blend films are generally smoother than the control binary films, as long as the **41** content is less than 10 wt%. The surface morphology of the ternary P3HT:$PC_{71}BM$:2.4 wt% **41** blend is the smoothest with a root mean square (RMS) roughness of ~8.26 nm. XRD results are in good agreement with the AFM images. Incorporating < 3.6 wt% **41** into the P3HT:$PC_{71}BM$ system enhances the intensity of the P3HT lamellar diffraction peak corresponding to the interchain spacing of P3HT, indicating that the crystalline packing of P3HT is enhanced on adding a small amount of **41**. However, incorporation of larger amounts of **41** into the film (> 3.6 wt%) result in decreased intensity of the P3HT diffraction peak. Both AFM images and XRD spectra indicate that low concentrations of **41** in the P3HT:$PC_{71}BM$ system do not substantially disturb the film morphology, while larger amounts of **41** are deleterious to the film morphology.

In 2017, Zhao and co-workers [129] investigated various ternary solar cells by incorporating the five squaraine derivatives **4** [71], **42** [130], **43** [131], **44** and **9** [82] into a poly[[9-(1-octylnonyl)-9H-carbazole-2,7-diyl]-2,5-thiophenediyl-2,1,3-benzothia-diazole-4,7-diyl-2,5-thiophenediyl] (PCDTBT):$PC_{71}BM$ host binary system. In a typical experiment, PCDTBT, $PC_{71}BM$ and the SQ are mixed in a weight ratio of 1:2:0.1 (the optimized composition), while the control binary blend contains PCDTBT and $PC_{71}BM$ in a weight ratio of 1:2. Solar cells of structure ITO/MoO_3/Active Layer/PFN/Al were then fabricated. The results show that the J_{SC} of the ternary devices with **4**, **42** and **43** exceeds 12 mA/cm^2 compared with 10.26 mA/cm^2 for the binary device, and the corresponding PCEs are 5.37%, 5.87% and 5.92%, respectively, thus showing >20% PCE enhancement compared with the PCDTBT:$PC_{71}BM$ binary device. Ternary solar cells incorporating **44** and **9** exhibit poor PCEs of 4.51% and 4.03%, respectively. To understand the performance difference, SCLC measurements were performed using ITO/MoO_3/Active layer/Au as hole-only and ITO/PFN/Active layer/Al as electron-only diodes, respectively. The μ_e / μ_h ratios are 3.37, 2.77, 2.27, 4.25, 5.18 for **4**, **42**, **43**, **44** and **9** containing ternary devices, respectively, versus 2.52 for the PCDTBT:$PC_{71}BM$ binary control cell. The larger μ_e / μ_h ratios for the **44** and **9** 10%-doped ternary devices point to reduced charge extraction and serious charge recombination in these devices, consistent with the FF trend of 50.09%, 51.68%, 52.16%, 47.76%, and 45.68%, respectively, and PCE of 5.37%, 5.87%, 5.92%, 4.51%, and 4.03%, respectively. The carrier recombination characteristics in the ternary devices were investigated by transient photovoltage (TPV) measurements. The charge carrier lifetime τ was determined by fitting the TPV signal with single-exponential decay. The charge carrier lifetime of binary device and **43**-based ternary devices are 22.5 μs and 23.2 μs, respectively, which falls to 13.6 μs when **9** is used as ternary component. The authors also measured charge carrier lifetimes of these devices at various V_{OC} condition. The result for the **43** based ternary device is almost identical to that of binary device under various V_{OC} conditions, while the carrier lifetime of the ternary device incorporated with **9** decreases dramatically, indicating more significant charge carrier recombination. Therefore, the mobility and TPV data clearly explain the solar cell performance, underscoring that both the absorption spectrum and energy levels of the added material must be considered in fabricating efficient ternary solar cells.

Finally and very recently (2018), this Laboratory [132] reported ternary solar cells by combining two squaraine

Table 2: Photovoltaic Performance Metrics of Squaraine-based Ternary Solar Cells

Device Structure	V_{oc} (V)	J_{sc} (mA cm^{-2})	FF	PCE (%)	Ref.
ITO/PEDOT:PSS / 9 wt% **4 :** PIDTDTQx:PCBM/PFN/Al	0.85	11.56	0.66	6.4	[127]
ITO/PEDOT:PSS / 2.4 wt% **41 :** P_3HT:$PC_{71}BM$/LiF/Al	0.56	11.31	0.62	3.93	[128]
ITO/ MoO_3/10% wt **4**: PCDTBT: $PC_{71}BM$ / PFN /Al	0.89	12.04	0.50	5.34	[129]
ITO/ MoO_3/10% wt **42**: PCDTBT: $PC_{71}BM$ / PFN /Al	0.90	12.63	0.52	5.73	[129]
ITO/ MoO_3/10% wt **43**: PCDTBT: $PC_{71}BM$ / PFN /Al	0.90	12.62	0.52	5.81	[129]
ITO/ MoO_3/10% wt **44**: PCDTBT: $PC_{71}BM$ / PFN /Al	0.87	10.86	0.48	4.31	[129]
ITO/ MoO_3/10% wt **9**: PCDTBT: $PC_{71}BM$ / PFN /Al	0.85	10.39	0.46	4.01	[129]
ITO/ MoO_3/ 15 wt% **40 : 29** :$PC_{71}BM$/LiF/Al	0.82	15.96	0.54	7.07	[132]

donors, **29** [105] and **40** [133], having complementary optical absorption with $PC_{71}BM$ as the acceptor. In the experiment, the weight ratio of **29**:$PC_{71}BM$ in the blend was maintained at 1:3 and different amounts of **40** versus **29** (in x wt% = 5, 10, 15, 20, 30%) were added, affording ternary blends of composition **40**:**29**:$PC_{71}BM$ = x:1:3 (x weight % = 0.05, 0.1, 0.15, 0.20, 0.30, respectively). The optimized ternary cells of weight composition **40**:**29**:$PC_{71}BM$ = 0.15:1.0:3.0 deliver a PCE as high as 7.20%, which is the highest value reported to date for a squaraine solar cell measured at 25ºC. As control, the corresponding binary cells exhibit a maximum PCE of 4.65% (**40** binary) and 6.85% (**29** binary) at 25ºC. This PCE difference between two binary cells is explained by the single crystal structure and SCLC measurements. For the ternary blends, SCLC measurements and transmission electron microscopy (TEM) imaging indicate that the charge mobility slightly increases and the BHJ domain size optimizes for the 0.15:1.0:3.0 ternary blend vs that based on the **29** blend. Grazing incidence wide-angle X-ray scattering (GIWAXS) data reveal that enhanced π-π stacking and larger correlation lengths can be achieved by thermal annealing of the ternary blend films, leading to the slight PCE enhancement (Figure 10). Charge recombination measurements show that **40** can be incorporated into the blend without increasing charge recombination. Overall, the **40**: **29**: $PC_{71}BM$ = 0.15:1.0:3.0 ternary devices have far greater and balanced mobilities and enhanced solar light absorption, resulting in enhanced OSC metrics. Finally, flexible solar cells on polyethylene terephthalate (PET) with a PCE of $\sim$ 4.5% were also fabricated. This study demonstrates that readily accessible squaraine cores represent a viable choice for the rational design of new organic solar cell donor materials.

6 Conclusions and prospective

We have reviewed the recent advances of SQ dyes and SQ dye-based solar cells since 2015, including molecular design and their applications on the binary/ternary solar cells. With impressive efforts by the SQ community, great advances have been achieved in recent years. Indoline and their derivatives are promising moieties for squaraine solar cells, and the central –OH substituent is an essential factor to preserve and enhance PCE. Moreover, enlarging the π-conjunction is another effective strategy for high-performance squaraine solar cells, which should be further emphasized in future molecular design. SQ as a third component incorporated with other semiconductors for ternary solar cells is another promising direction for SQ solar cells.

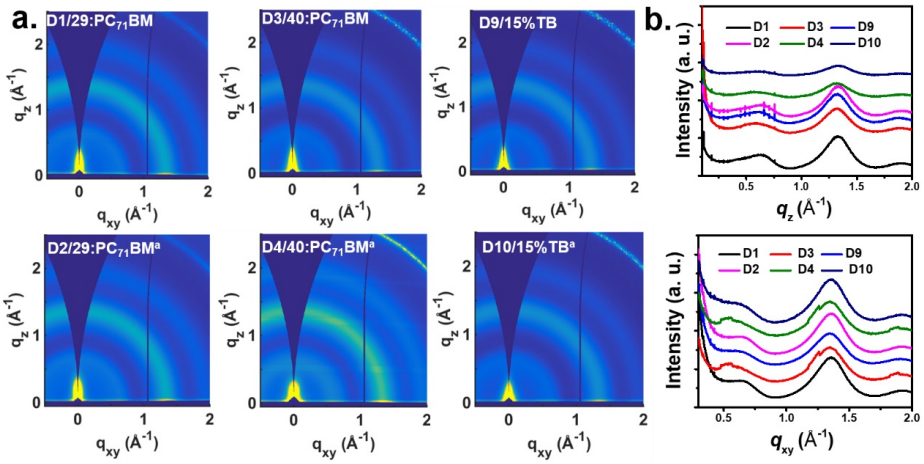

Fig. 10: (a) Two-dimensional (2D) GIWAXS images of the indicated blend films. (b) Corresponding in-plane and out-of-plane line cuts. [a]The active layer was annealed at 80°C for 10 min [132]. Reprinted with permission from Ref. [132]. Copyright 2018 American Chemical Society.

However, the PCEs of squaraine OSCs is still far behind of the state-of-the-art in organic solar energy conversion, especially in view of the recent advances in polymeric nonfullerene solar cells. To further enhance the PCEs of SQ solar cells, the critical issue is still the hole mobility. Higher charge mobilities could lead to better J_{SC} and FF metrics. It noteworthy that the modest FFs ($\sim$ 0.50) of SQ solar cells is a key bottleneck for improving PCEs in these devices. Materials design and morphology optimization are routes to achieve high carrier mobility devices. Furthermore, it is essential to explore with greater efforts the performance of SQ solar cells fabricated with nonfullerene acceptors. With these issues addressed properly, greater PCEs can be expected for SQ solar cells in the future.

Acknowledgement: This work was supported in part by the Center for Light Energy Activated Redox Processes (LEAP), an Energy Frontier Research Center funded by the U.S. Department of Energy, Office of Science, Office of Basic Energy Sciences under Award DE-SC0001059, AFOSR grant FA9550-18-1-0320, the Northwestern University Materials Research Science and Engineering Center under NSF grant DMR-1720139, and Flexterra Corp.

References

[1] A. J. McEvoy, L. Castaner, T. Markvart, *Solar cells: materials, manufacture and operation*, Academic Press, 2012.
[2] M. A. Green, K. Emery, Y. Hishikawa, W. Warta, E. D. Dunlop, Progress in Photovoltaics: Research and Applications 2016, 24, 905.
[3] A. F. Paterson, N. D. Treat, W. Zhang, Z. Fei, G. Wyatt-Moon, H. Faber, G. Vourlias, P. A. Patsalas, O. Solomeshch, N. Tessler, M. Heeney, T. D. Anthopoulos, Adv. Mater. 2016, 28, 7791.
[4] A. Facchetti, Chem. Mater. 2011, 23, 733.
[5] L. Lu, T. Zheng, Q. Wu, A. M. Schneider, D. Zhao, L. Yu, Chem. Rev. 2015, 115, 12666.
[6] Y.-J. Cheng, S.-H. Yang, C.-S. Hsu, Chem. Rev. 2009, 109, 5868.
[7] Y. Z. Lin, P. Cheng, Y. Liu, Q. Q. Shi, W. P. Hu, Y. F. Li, X. W. Zhan, Org. Electron. 2012, 13, 673.
[8] L. Dou, Y. Liu, Z. Hong, G. Li, Y. Yang, Chem. Rev. 2015, 115, 12633.
[9] F. C. Krebs, N. Espinosa, M. Hösel, R. R. Søndergaard, M. Jørgensen, Adv. Mater. 2014, 26, 29.
[10] Y. Lin, X. Zhan, Acc. Chem. Res. 2015, 49, 175.
[11] G. Yu, A. J. Heeger, J. Appl. Phy. 1995, 78, 4510.
[12] G. Yu, J. Gao, J. C. Hummelen, F. Wudl, A. J. Heeger, Science 1995, 270, 1789.
[13] J. Halls, C. Walsh, N. Greenham, E. Marseglia, R. Friend, S. Moratti, A. Holmes, Nature 1995, 376, 498.
[14] Y. He, Y. Li, Phy. Chem. Chem. Phy. 2011, 13, 1970.
[15] Y.-Y. Lai, Y.-J. Cheng, C.-S. Hsu, Energy Environ. Sci. 2014, 7, 1866.
[16] Z. He, B. Xiao, F. Liu, H. Wu, Y. Yang, S. Xiao, C. Wang, T. P. Russell, Y. Cao, Nat. Photonics 2015, 9, 174.
[17] Y. Liu, J. Zhao, Z. Li, C. Mu, W. Ma, H. Hu, K. Jiang, H. Lin, H. Ade, H. Yan, Nat. Comm. 2014, 5, 5293.
[18] J. Zhao, Y. Li, G. Yang, K. Jiang, H. Lin, H. Ade, W. Ma, H. Yan, Nat. Energy 2016, 1, 15027.
[19] Y. He, H.-Y. Chen, J. Hou, Y. Li, J. Am. Chem. Soc. 2010, 132, 1377.
[20] M. Jørgensen, K. Norrman, S. A. Gevorgyan, T. Tromholt, B. Andreasen, F. C. Krebs, Adv. Mater. 2012, 24, 580.
[21] A. Distler, T. Sauermann, H. J. Egelhaaf, S. Rodman, D. Waller, K. S. Cheon, M. Lee, D. M. Guldi, Adv. Energy Mater. 2014, 4, 1300693.
[22] P. Cheng, C. Yan, T. K. Lau, J. Mai, X. Lu, X. Zhan, Adv. Mater. 2016, 8, 5822.
[23] P. Cheng, C. Yan, Y. Wu, J. Wang, M. Qin, Q. An, J. Cao, L. Huo, F. Zhang, L. Ding, Adv. Mater. 2016, 28, 8021.
[24] X. Zhan, Z. a. Tan, B. Domercq, Z. An, X. Zhang, S. Barlow, Y. Li, D. Zhu, B. Kippelen, S. R. Marder, J. Am. Chem. Soc. 2007,

129, 7246.
[25] J. Zhang, H. S. Tan, X. Guo, A. Facchetti, H. Yan, Nat. Energy 2018, 3, 720.
[26] Z. Li, L. Ying, P. Zhu, W. Zhong, N. Li, F. Liu, F. Huang, Y. Cao, Energy Environ. Sci. 2019, 12, 157.
[27] G. Wang, F. S. Melkonyan, A. Facchetti, T. J. Marks, Angew. Chem. Int. Ed. 2019, 131, 4173.
[28] H. Yan, Z. Chen, Y. Zheng, C. Newman, J. R. Quinn, F. Dotz, M. Kastler, A. Facchetti, Nature 2009, 457, 679.
[29] M. M. Durban, P. D. Kazarinoff, C. K. Luscombe, Macromolecules 2010, 43, 6348.
[30] T. Kim, J. Choi, H. J. Kim, W. Lee, B. J. Kim, Macromolecules 2017, 50, 6861.
[31] T. Kim, R. Younts, W. Lee, S. Lee, K. Gundogdu, B. J. Kim, J. Mater. Chem. A 2017, 5, 22170.
[32] T. Kim, J.-H. Kim, T. E. Kang, C. Lee, H. Kang, M. Shin, C. Wang, B. Ma, U. Jeong, T.-S. Kim, B. J. Kim, Nat. Commun. 2015, 6, 8547.
[33] Y. Guo, Y. Li, O. Awartani, J. Zhao, H. Han, H. Ade, D. Zhao, H. Yan, Adv. Mater. 2016, 28, 8483.
[34] N. Zhou, A. Facchetti, Materials Today 2018, 21, 377.
[35] C. Dou, X. Long, Z. Ding, Z. Xie, J. Liu, L. Wang, Angew. Chem. Int. Ed. 2016, 55, 1436.
[36] X. Long, Z. Ding, C. Dou, J. Zhang, J. Liu, L. Wang, Adv. Mater. 2016, 28, 6504.
[37] S. V. Bhosale, S. V. Bhosale, S. K. Bhargava, Org. Biomol. Chem. 2012, 10, 6455.
[38] M. A. Kobaisi, S. V. Bhosale, K. Latham, A. M. Raynor, S. V. Bhosale, Chem. Rev. 2016, 116, 11685.
[39] Q. Yan, Y. Zhou, Y.-Q. Zheng, J. Pei, D. Zhao, Chem. Sci. 2013, 4, 4389.
[40] R. A. Street, T. N. Ng, R. A. Lujan, I. Son, M. Smith, S. Kim, T. Lee, Y. Moon, S. Cho, ACS Appl. Mater. Interfaces 2014, 6, 4428.
[41] S. Rajaram, R. Shivanna, S. K. Kandappa, K. Narayan, J. Phy. Chem. Lett. 2012, 3, 2405.
[42] X. Zhang, Z. Lu, L. Ye, C. Zhan, J. Hou, S. Zhang, B. Jiang, Y. Zhao, J. Huang, S. Zhang, Adv. Mater. 2013, 25, 5791.
[43] W. Jiang, L. Ye, X. Li, C. Xiao, F. Tan, W. Zhao, J. Hou, Z. Wang, Chem. Comm. 2014, 50, 1024.
[44] Y. Zang, C. Z. Li, C. C. Chueh, S. T. Williams, W. Jiang, Z. H. Wang, J. S. Yu, A. K. Jen, Adv. Mater. 2014, 26, 5708.
[45] Y. Liu, C. Mu, K. Jiang, J. Zhao, Y. Li, L. Zhang, Z. Li, J. Y. Lai, H. Hu, T. Ma, R. Hu, D. Yu, X. Huang, B. Z. Tang, H. Yan, Adv. Mater. 2015, 27, 1015.
[46] Y. Lin, X. Zhan, Acc. Chem. Res. 2016, 49, 175.
[47] J. Liu, S. Chen, D. Qian, B. Gautam, G. Yang, J. Zhao, J. Bergqvist, F. Zhang, W. Ma, H. Ade, O. Inganäs, K. Gundogdu, F. Gao, H. Yan, Nat. Energy 2016, 1, 16089.
[48] S. Li, L. Ye, W. Zhao, S. Zhang, S. Mukherjee, H. Ade, J. Hou, Adv. Mater. 2016, 28, 9423.
[49] W. Zhao, D. Qian, S. Zhang, S. Li, O. Inganas, F. Gao, J. Hou, Adv. Mater. 2016, 28, 4734.
[50] J. Yao, T. Kirchartz, M. S. Vezie, M. A. Faist, W. Gong, Z. He, H. Wu, J. Troughton, T. Watson, D. Bryant, J. Nelson, Phy. Rev. Appl. 2015, 4, 014020.
[51] T. J. Aldrich, S. M. Swick, F. S. Melkonyan, T. J. Marks, Chem. Mater. 2017, 29, 10294.
[52] C. Yan, S. Barlow, Z. Wang, H. Yan, A. K. Y. Jen, S. R. Marder, X. Zhan, Nat. Rev. Mater. 2018, 3, 18003.
[53] B. Fan, D. Zhang, M. Li, W. Zhong, Z. Zeng, L. Ying, F. Huang, Y. Cao, Sci. China Chem. 2019, DOI: 10.1007/s11426-019-9457-5.
[54] S. D. Collins, N. A. Ran, M. C. Heiber, T.-Q. Nguyen, Adv. Energy Mater. 2017, 7, 1602242.
[55] M. Riede, T. Mueller, W. Tress, R. Schueppel, K. Leo, Nanotechnology 2008, 19, 424001/1.
[56] B. Kan, M. Li, Q. Zhang, F. Liu, X. Wan, Y. Wang, W. Ni, G. Long, X. Yang, H. Feng, Y. Zuo, M. Zhang, F. Huang, Y. Cao, T. P. Russell, Y. Chen, J. Am. Chem. Soc. 2015, 137, 3886.
[57] D. Deng, Y. Zhang, J. Zhang, Z. Wang, L. Zhu, J. Fang, B. Xia, Z. Wang, K. Lu, W. Ma, Z. Wei, Nat. Comm. 2016, 7, 13740.
[58] J. Yang, F. Chen, B. Xiao, S. Sun, X. Sun, K. Tajima, A. Tang, E. Zhou, Solar RRL 2018, 2.
[59] K. Gao, S. B. Jo, X. Shi, L. Nian, M. Zhang, Y. Kan, F. Lin, B. Kan, B. Xu, Q. Rong, L. Shui, F. Liu, X. Peng, G. Zhou, Y. Cao, A. K. Y. Jen, Adv. Mater. 2019.
[60] G. Chen, H. Sasabe, T. Igarashi, Z. R. Hong, J. Kido, J. Mater. Chem. A 2015, 3, 14517.
[61] D. Bagnis, L. Beverina, H. Huang, F. Silvestri, Y. Yao, H. Yan, G. A. Pagani, T. J. Marks, A. Facchetti, J. Am. Chem. Soc. 2010, 132, 4074.
[62] M. Sassi, M. Crippa, R. Ruffo, R. Turrisi, M. Drees, U. K. Pandey, R. Termine, A. Golemme, A. Facchetti, L. Beverina, J. Mater. Chem. A 2013, 1, 2631.
[63] R. Turrisi, L. Mascheroni, M. Sassi, M. Rooney, N. Buccheri, R. Ruffo, A. Facchetti, L. Beverina, Eur. J. Org. Chem. 2016, 2016, 4032.
[64] A. Broggi, H. Kim, J. Jung, M. P. Bracciale, M. L. Santarelli, C. Kim, A. Marrocchi, Macromol. Chem. Phys. 2017, 218, 1600487.
[65] D. Yang, Z. Guan, L. Yang, Y. Huang, Q. Wei, Z. Lu, J. Yu, Sol. Energy Mater. Sol. Cells 2012, 105, 220.
[66] T. Maeda, T. Tsukamoto, A. Seto, S. Yagi, H. Nakazumi, Macromolecular Chem. Phys. 2012, 213, 2590.
[67] S. F. Völker, S. Uemura, M. Limpinsel, M. Mingebach, C. Deibel, V. Dyakonov, C. Lambert, Macromolecular Chem. Phys. 2010, 211, 1098.
[68] V. Y. Merritt, H. J. Hovel, App. Phy. Lett. 1976, 29, 414.
[69] F. Silvestri, M. D. Irwin, L. Beverina, A. Facchetti, G. A. Pagani, T. J. Marks, J. Am. Chem. Soc. 2008, 130, 17640.
[70] U. Mayerhoffer, K. Deing, K. Gruss, H. Braunschweig, K. Meerholz, F. Würthner, Angew. Chem. Int. Ed. 2009, 48, 8776.
[71] S. Wang, E. I. Mayo, M. D. Perez, L. Griffe, G. Wei, P. I. Djurovich, S. R. Forrest, M. E. Thompson, App. Phy. Lett. 2009, 94, 233304.
[72] G. Wei, R. R. Lunt, K. Sun, S. Wang, M. E. Thompson, S. R. Forrest, Nano letters 2010, 10, 3555. ü
[73] G. Wei, S. Wang, K. Sun, M. E. Thompson, S. R. Forrest, Adv. Energy Mater. 2011, 1, 184.
[74] G. Chen, H. Sasabe, Z. Wang, X. F. Wang, Z. Hong, Y. Yang, J. Kido, Adv. Mater. 2012, 24, 2768.
[75] B. E. Lassiter, J. D. Zimmerman, A. Panda, X. Xiao, S. R. Forrest, App. Phys. Lett. 2012, 101.
[76] B. Fan, Y. Maniglio, M. Simeunovic, S. Kuster, T. Geiger, R. Hany, F. Nuesch, International Journal of Photoenergy 2009, 2009, 1.
[77] G. Wei, X. Xiao, S. Wang, K. Sun, K. J. Bergemann, M. E. Thompson, S. R. Forrest, ACS Nano 2012, 6, 972.

[78] J. D. Zimmerman, B. E. Lassiter, X. Xiao, K. Sun, A. Dolocan, R. Gearba, D. A. Vanden Bout, K. J. Stevenson, P. Wickramasinghe, M. E. Thompson, S. R. Forrest, ACS Nano 2013, 7, 9268.
[79] D. Yang, Q. Yang, L. Yang, Q. Luo, Y. Chen, Y. Zhu, Y. Huang, Z. Lu, S. Zhao, Chem. Comm. 2014, 50, 9346.
[80] D. Yang, Q. Yang, L. Yang, Q. Luo, Y. Huang, Z. Lu, S. Zhao, Chem. Comm. 2013, 49, 10465.
[81] L. Yang, Q. Q. Yang, D. B. Yang, Q. Luo, Y. Q. Zhu, Y. Huang, S. L. Zhao, Z. Y. Lu, J. Mater. Chem. A 2014, 2, 18313.
[82] Y. Chen, Y. Zhu, D. Yang, Q. Luo, L. Yang, Y. Huang, S. Zhao, Z. Lu, Chem. Comm. 2015, 51, 6133.
[83] L. Beverina, P. Salice, Eur. J. Org. Chem. 2010, 1207.
[84] L. Hu, Z. Yan, H. Xu, RSC Adv. 2013, 3, 7667.
[85] D. E. Lynch, D. G. Hamilton, J. Heterocycl. Chem. 2018, 55, 1249.
[86] S. Sreejith, P. Carol, P. Chithra, A. Ajayaghosh, J. Mater. Chem. 2008, 18, 264.
[87] H. E. Sprenger, Ziegenbe.W, Angew. Chem. Int. Ed. 1968, 7, 530.
[88] K. Y. Law, F. C. Bailey, J. Org. Chem. 1992, 57, 3278.
[89] L. Beverina, P. Salice, Eur. J. Org. Chem. 2010, 2010, 1207.
[90] G. M. Xia, H. M. Wang, Journal of Photochemistry and Photobiology C-Photochemistry Reviews 2017, 31, 84.
[91] L. S. Liebeskind, R. W. Fengl, J. Org. Chem. 1990, 55, 5359.
[92] S. Yagi, T. Ohta, N. Akagi, H. Nakazumi, Dyes Pigm.2008, 77, 525.
[93] V. Rapozzi, L. Beverina, P. Salice, G. A. Pagani, M. Camerin, L. E. Xodo, J. Med. Chem. 2010, 53, 2188.
[94] D. Yang, H. Sasabe, T. Sano, J. Kido, ACS Energy Letters 2017, 2, 2021.
[95] D. Yang, Y. Jiao, L. Yang, Y. Chen, S. Mizoi, Y. Huang, X. Pu, Z. Lu, H. Sasabe, J. Kido, J. Mater. Chem. A 2015, 3, 17704.
[96] Z. Chen, J. Brown, M. Drees, M. Seger, Y. Hu, Y. Xia, D. Boudinet, M. McCray, M. Delferro, T. J. Marks, C.-Y. Liao, C.-W. Ko, Y.-M. Chang, A. Facchetti, Chem. Mater. 2016, 28, 6390.
[97] D. Yang, L. Yang, Y. Huang, Y. Jiao, T. Igarashi, Y. Chen, Z. Lu, X. Pu, H. Sasabe, J. Kido, ACS Appl. Mater. Interfaces 2015, 7, 13675.
[98] Y. Chen, G. Wang, L. Yang, J. Wu, F. S. Melkonyan, Y. Huang, Z. Lu, T. J. Marks, A. Facchetti, J. Mater. Chem. C 2018, 6, 847.
[99] S. Paek, H. Choi, H. Jo, K. Lee, K. Song, S. A. Siddiqui, G. D. Sharma, J. Ko, J. Mater. Chem. C 2015, 3, 7029.
[100] Y. Lin, X. Zhan, Acc. Chem. Res. 2016, 49, 175.
[101] D. Yang, H. Sasabe, Y. Jiao, T. Zhuang, Y. Huang, X. Pu, T. Sano, Z. Lu, J. Kido, J. Mater. Chem. A 2016, 4, 18931.
[102] C. M. Proctor, J. A. Love, T. Q. Nguyen, Adv. Mater. 2014, 26, 5957.
[103] Q. Xiao, Y. Li, F. Wu, M. Han, M. Xie, Z. Li, L. Zhu, Z. a. Li, J. Mater. Chem. C 2018, 6, 10547.
[104] G. Chen, H. Sasabe, Y. Sasaki, H. Katagiri, X. F. Wang, T. Sano, Z. R. Hong, Y. Yang, J. Kido, Chem. Mater. 2014, 26, 1356.
[105] J. Wu, C. Si, Y. Chen, L. Yang, B. Hu, G. Chen, Z. Lu, Y. Huang, Chem. Eur. J. 2018, 24, 3234.
[106] J. Wu, D. Yang, Q. Wang, L. Yang, H. Sasabe, T. Sano, J. Kido, Z. Lu, Y. Huang, J. Mater. Chem. A 2018, 6, 5797.
[107] Y. Chen, Y. Zhu, D. Yang, S. Zhao, L. Zhang, L. Yang, J. Wu, Y. Huang, Z. Xu, Z. Lu, Chem. Eur. J 2016, 22, 14527.
[108] G. Wei, S. Wang, K. Sun, M. E. Thompson, S. R. Forrest, Adv. Energy Mater. 2011, 1, 184.
[109] S. Y. Wang, L. Hall, V. V. Diev, R. Haiges, G. D. Wei, X. Xiao, P. I. Djurovich, S. R. Forrest, M. E. Thompson, Chem. Mater. 2011, 23, 4789.
[110] L. Yang, Y. Zhu, Y. Jiao, D. Yang, Y. Chen, J. Wu, Z. Lu, S. Zhao, X. Pu, Y. Huang, Dyes Pigm. 2017, 145, 222.
[111] L. Yang, D. B. Yang, Y. Chen, Q. Luo, M. G. Zhang, Y. Huang, Z. Y. Lu, H. Sasabe, J. Kido, Rsc Advances 2016, 6, 1877.
[112] Y. Chen, J. Wu, L. Yang, B. Hu, D. Yang, Z. Lu, Y. Huang, Chem. Eur. J. 2018, 24, 8747.
[113] L. Yang, D. Yang, Y. Chen, J. Wu, Z. Lu, H. Sasabe, J. Kido, T. Sano, Y. Huang, Mater. Chem. Front. 2018, 2, 2116.
[114] T. Ameri, P. Khoram, J. Min, C. J. Brabec, Adv. Mater. 2013, 25, 4245.
[115] Y. F. Zhao, L. Yuan, J. Q. Zhang, L. Y. Zhu, K. Lu, W. Yan, Z. X. Wei, RSC Advances 2015, 5, 61703.
[116] Q. An, F. Zhang, J. Zhang, W. Tang, Z. Deng, B. Hu, Energy Environ. Sci. 2016, 9, 281.
[117] J. Wang, F. J. Zhang, J. Xiao, F. Li, M. Zhang, Q. S. An, J. Zhang, J. Mater. Chem. C 2016, 4, 7809.
[118] S. V. Dayneko, A.-J. Payne, G. C. Welch, Can. J. Chem. 2018, 96, 703.
[119] T. Goh, J. S. Huang, K. G. Yager, M. Y. Sfeir, C. Y. Nam, X. Tong, L. M. Guard, P. R. Melvin, F. Antonio, B. G. Bartolome, M. L. Lee, N. Hazari, A. D. Taylor, Adv. Energy Mater. 2016, 6, 1600660.
[120] M. Zhang, J. Wang, F. Zhang, Y. Mi, Q. S. An, W. B. Wang, X. L. Ma, J. Zhang, X. F. Liu, Nano Energy 2017, 39, 571.
[121] Q. S. An, F. J. Zhang, Q. Q. Sun, M. Zhang, J. Zhang, W. H. Tang, X. X. Yin, Z. B. Deng, Nano Energy 2016, 26, 180.
[122] K. Feron, J. M. Cave, M. N. Thameel, C. O'Sullivan, R. Kroon, M. R. Andersson, X. Zhou, C. J. Fell, W. J. Belcher, A. B. Walker, P. C. Dastoor, ACS App. Mater. Interfaces 2016, 8, 20928.
[123] J. Kong, M. M. Beromi, M. Mariano, T. Goh, F. Antonio, N. Hazari, A. D. Taylor, Nano Energy 2017, 38, 36.
[124] Y. Zhu, L. Yang, S. Zhao, Y. Huang, Z. Xu, Q. Yang, P. Wang, Y. Li, X. Xu, Phy. Chem. Chem. Phy. 2015, 17, 26777.
[125] T. Goh, J. S. Huang, E. A. Bielinski, B. A. Thompson, S. Tomasulo, M. L. Lee, M. Y. Sfeir, N. Hazari, A. D. Taylor, ACS Photo. 2015, 2, 86.
[126] Y. F. Zheng, J. Huang, G. Wang, J. M. Kong, D. Huang, M. M. Beromi, N. Hazari, A. D. Taylor, J. S. Yu, Materials Today 2018, 21, 79.
[127] M. Zhang, F. Zhang, Q. An, Q. Sun, J. Wang, L. Li, W. Wang, J. Zhang, Sol. Energy Mater. Sol. Cells 2015, 141, 154.
[128] L. Zhu, R. Wang, J. Qiao, F. Wu, Dyes Pigm. 2016, 132, 20.
[129] Y. Zhu, Y. Chen, S. Zhao, Y. Huang, Z. Xu, B. Qiao, J. Zhao, Y. Li, J. Liu, X. Xu, Synth. Met. 2017, 234, 125.
[130] A. M. Della Pelle, P. J. Homnick, Y. Bae, P. M. Lahti, S. Thayumanavan, J. Phys. Chem. C 2014, 118, 1793.
[131] H. Sasabe, T. Igrashi, Y. Sasaki, G. Chen, Z. Hong, J. Kido, RSC Advances 2014, 4, 42804.
[132] Y. Chen, L. Yang, J. Wu, G. Wang, W. Huang, F. S. Melkonyan, Z. Lu, Y. Huang, T. J. Marks, A. Facchetti, Chem. Mater. 2018, 30, 6810.
[133] D. Yang, T. Sano, H. Sasabe, L. Yang, S. Ohisa, Y. Chen, Y. Huang, J. Kido, ACS Appl. Mater. Interfaces 2018, 10, 26465.